OPEN ACCESS Freely available online

Andrology: Open Access

Research Article

Concomitant Increases in Both Prostate Gland and Blood Serum VEGF Levels at the Onset of Rat Age Related Benign Hyperplasia would be Related with an Increase in Both Processing and Secretion of Prostatic VEGF

Trujillo-Rojas L[1,2], Fernández-Novell JM[3], Blanco-Prieto O[1,4], Rigau T[1], Rivera del Álamo MM[1], Rodríguez-Gil JE[1*]

[1]Department of Animal Medicine and Surgery, Autonomous University of Barcelona, Bellaterra, Spain; [2]Department of Veterinary Medicine, University of Pamplona, Pamplona, Colombia; [3]Department of Biochemistry and Molecular Biology, University of Barcelona, Barcelona, Spain; [4]Department of Veterinary Medical Sciences, University of Bologne, Bologna, Italy

ABSTRACT

Our research team recently demonstrated that the onset of rat age-related Benign Prostatic Hyperplasia (BPH) is concomitant with parallel increases of both prostatic and blood serum Vascular Endothelial Growth Factor (VEGF) levels. This follow up was centered in how prostatic expression and location of VEGF modify depending on the BPH onset was raised. To evaluate this, prostatic expression and location of both VEGF and its specific receptor (VEGF-R) were analyzed by both Western blot and immunohistochemistry in rats with separate ages. Results indicate that VEGF significantly ($P<0.05$) increased its prostate expression in BPH-affected rats, being this increase parallel with a change in the intracellular VEGF location, which went from a per membranous situation in healthy animals to an intracytoplasmic one in BPH-affected ones. Moreover, there was evidence of a Golgi apparatus-related location of VEGF in BPH animals. In all, results seem indicate that the observed concomitant BPH-related changes in prostatic tissue and blood serum VEGF levels would be related with an increase in both prostate, Golgi apparatus-related VEGF processing and further extracellular secretion.

Keywords: Benign prostatic hyperplasia; VEGF; Rat; Western blot

INTRODUCTION

Benign prostatic hyperplasia (BPH) is a well-known age-related process that affects species such as human and rodents [1-3]. Although BPH is inherently a benign process, its importance lays not only in the appearance of annoying symptomatology, such as urinary discomfort, but also in being considered as a first step in the pathological way leading to the appearance of prostatic neoplasia [4-9]. In this way, a precise knowledge regarding BPH pathogenesis is essential to develop better tools for the prognosis of severe prostatic alterations. In the last years, inflammation has been described as one of the most important triggers, if not the most, of BPH [10-13]. Thus, the role of chemokines, including vasculogenic factors, in the onset of BPH has been well established [14]. This is an important asset when considering that these factors also play a key role in the further development of prostatic tumors [4-8]. In fact, vasculogenic factors are especially important since vasculogenesis plays a key role in cell proliferation leading firstly to BPH and, subsequently, to prostatic tumors [15,16]. Several studies have shown that angiogenic factors such as the endothelial vascular growth factor (VEGF), the Fibroblasts Growth Factor 1 (FGF-1) and 2 (FGF-2), several metalloproteinases, the Insulin-like Growth Factor I (IGF-I) and the angiopoietin modulate neovascularization through complex autocrine and paracrine mechanisms during the onset of BPH and subsequent prostatic tumors [15-17]. From all these factors, VEGF seems to play a distinguished role, being already described to be involved in the development of prostatic carcinoma [18]. This assert has been further supported by data obtained in our laboratory indicating that the onset of rat BPH is concomitant with parallel increases of both prostatic and blood serum VEGF

Correspondence to: Rodríguez-Gil JE, Department of Animal Medicine and Surgery, Autonomous University of Barcelona, Bellaterra, Spain, Tel: +34-935811045; E-mail: juanenrique.rodriguez@uab.cat

Received: 11-Feb-2022, Manuscript No. ANO-22-15897; **Editor assigned:** 14-Feb-2022, PreQC No. ANO-22-15897(PQ); **Reviewed:** 28-Feb-2022, QC No. ANO-22-15897; **Revised:** 07-Mar-2022, Manuscript No. ANO-22-15897(R); **Published:** 14-Mar-2022, DOI:10.35248/2167-0250.22.S1.003.

Citation: Rojas LT, Novell JMF, Prieto OB, Rigau T, Álamo MMRD,Gil JER (2022) Concomitant Increases in Both Prostate Gland and Blood Serum VEGF Levels at the Onset of Rat Age Related Benign Hyperplasia would be Related with an Increase in Both Processing and Secretion of Prostatic VEGF. Andrology. S1:003.

levels [19]. However, the exact mechanisms by which VEGF exert its vasculogenic effects on prostate gland are not well known. Thus, although several reports suggest a direct action of VEGF through its canonical receptors, which are present in endothelial cells (VEGF-R) [20], other authors described an androgen-dependent mechanism through the formation of a Golgi apparatus-modulated in tumor prostatic cells, VEGF-androgen-androgen receptor-Specific Protein 1 (Sp1) complex [18]. This latter mechanism has not been described in BPH so far, although the existence of two independent mechanisms for the VEGF action could explain the published discrepancies regarding the expression of VEGF in both BPH and prostatic carcinoma. In this way, whereas several authors found significant differences in the prostatic expression of VEGF between BPH and prostatic carcinoma, other authors indicated that these differences were mainly due to intrinsic differences among samples and even among the utilized detection techniques [15-17]. All of these data pointed out to that, although the relationship between VEGF and the onset of BPH seems clear, there is not a depth knowledge concerning the previous evolution of VEGF expression, as well as that of canonical VEGF-R during the process that would eventually lead to the onset of BPH. Taking all this information into account, the main aim of this work was to analyze the evolution of the expression, through Western blot and immunocytochemistry, of VEGF and VEGF-R linked with the onset of BPH in rats. For this purpose, prostate glands from rats of different ages (1 month, 3 months, 6 months and 12 months) were analyzed to determine the putative age-related changes in the expression of both VEGF and VEGF-R. Moreover, putative, parallel changes in both the co-location of VEGF and Golgi apparatus, which could suggest the presence of a non-canonical pathway for VEGF action. To go further in depth in the knowledge of the putative role of VEGF in the onset of BPH.

MATERIALS AND METHODS

Animals

In this study, 28 healthy Sprague Dawley male rats aged 1 month-old (prepuberal, n=7), 3 months-old (pubertal, n=7), 6 months-old (mature, n=7) and 12 months-old (elder,n=7) were used. Animals were directly purchased from a commercial supplier (Harlan Interfauna Ibérica S.L., Sant Feliu de Codines, Spain) at the indicated ages. Once at the laboratory, animals were housed at the University facilities under controlled environmental conditions (12 h/12 h light darkness cycle, 20°C and 40% humidity) for 48 h, where they were fed with a commercial diet and water "ad libitum". Next morning after the 48 h-period, rats were euthanatized by introduction in a CO_2 chamber for 5 min. Once death was determined, blood samples were immediately obtained through intracardiac puncture and ventral prostatic lobe was removed through a celiotomy. Blood samples were allowed to clot at 20°C for 20 min and subsequently centrifuged at 1600 xg at 4°C for 10 min. afterwards, serums samples were recovered and immediately frozen in liquid N_2. Frozen serum samples were then stored at -80°C until their use. Regarding prostatic tissues, after a careful dissection, the obtained ventral prostatic lobes were excised into two portions. The first portion was fixed in a 4% (v:v) formaldehyde solution in phosphate buffered saline (PBS, pH 7.4) at 20°C at a volume proportion of 10:1. Samples were kept inside the formaldehyde solutions for a minimum of 24 h at 20°C before their use. These fixed portions were used to perform histological and immunohistological analyses. On the other side, the second portion was immediately frozen in liquid N_2 and subsequently stored at -80°C. Frozen sections were utilized for immunoblotting analyses. This experimental design did not require any specific code from the Ethical Commission (EC) of the Autonomous University of Barcelona (AUB), since there was no experimental procedure linked to the work. In any case, our procedure was specifically approved by the EC of the AUB, following the Animal Welfare Guidelines approved by both the Spanish and Catalan Governments.

Processing samples for histological and immunohistological procedures

Histological Hematoxylin-Eosin (H-E) staining of prostatic tissue samples was performed on formaldehyde-fixed samples that were thoroughly washed with PBS and then dehydrated through sequential immersion in ethanol dilutions from 70% (v:v) to 100% (v:v), following standard practices. Once dehydrated, samples were subsequently submerged in xylol for 1h at 20°C and then embedded in paraffin overnight at 58°C. The obtained paraffined samples were subsequently cooled at 4°C and a solid block was formed (approximate time: 1h). These blocks were subsequently sliced with a microtome (HistoCore Biocat®; Leica Biosystems; Wetzlar, Germany). Obtained slices had thickness of both 5 µm and 7 µm. Finally, obtained slices were placed onto 25 mm × 75 mm xylene-coated slides prior staining. Slides stained with Haematoxylin-Eosin (H-E) staining were used to evaluate the histology of the sample. Immunohistochemistry against both VEGF and VEGF receptor as well as specific markings of Golgi apparatus was also performed on formaldehyde-fixed samples that were thoroughly washed with PBS. Afterwards, samples were treated with sequential immersion in hydrous dilutions of sacarose from 5% (w:v) to 30 % (w:v), following standard practices. Afterwards, samples were embedded in the cry inclusion medium OCT Tissue-Tek® (Sakura Finetek; Tokio, Japan). When embedding was completed, samples were stored at -20°C until a solid block was formed (approximate time: 3-4h). Frozen, solid blocks were subsequently sliced through a cryostat (Leica CM3050 S; Leica Biosystems) to obtain slices with a thickness of 20 µm. These slices were placed onto 25 mm × 75 mm xylene-coated slides and stored at -20°C until their use.

Immunoblotting of prostatic tissue

For this analysis, frozen prostate samples were homogenized in an ice-cold homogenization buffer. This buffer was different depending on the specific analyzed protein. Thus, for VEGF immunoblotting, samples were homogenized in a 50 mM Tris/HCl buffer (pH 7.4) added with 1mM EDTA, 1% (v:v), 10mM ethyleneglycil-bis-(2-aminoethyleter)-N,N,N',N' tetra acetic acid (EGTA), 25 mM Dithiothreitol (DTT), 1.5 (v/v) Triton X-100®, 1mM phenylmethylsulfonyl fluoride (PMSF),

10 µg/mL leupeptin,1mM Na_2VO_4 and 1 mM benzamine (H Buffer). On the other hand, samples utilized for the detection of the VEGF-R were homogenized in a 50 mm Tris/HCl buffer (pH 7.5) added with 1mM Ethylene Diamante Traacetic acid (EDTA), 1% (v:v) Nonidet P-40®, 0.25% (w:v) sodium deoxycolate, 0.05% (w:v) sodium dodecyl sulfate (SDS), 150 mM NaCl, 1mM PMSF, 10 µg/mL leupeptin, 1 mM Na_2VO_4 and 1 mM benzamine (RIPA Buffer). Differences in the homogenization buffers between VEGF and VEGF-R were due to the separate location of both proteins, in cell cytosol of membranes, seeking thus for the most optimal buffer for each case. The homogenization buffer/prostate sample ratio was in all cases of 1µg tissue/5 µL buffer. Homogenization was carried out by using an Ultra-Turrax® T25 Basic homogenizer (IKA®-Werke; Staufen, Germany) at a homogenization velocity of 13500 r.p.m. for approximately 1 min. Once assured that samples were completely homogenized, they were centrifuged at 1200 xg for 10 min at 4°C and obtained supernatants were collected for immunoblotting. For this purpose, the first step was the analysis of the total protein content of samples through the Braford technique [21], by Using a commercial kit (BioRad; Hercules, CA, USA). Afterwards, samples were subjected to a polyacrylamide gel electrophoresis procedure in the presence of SDS (SDS-PAGE) as described in [22]. In all cases, the total protein content loaded in each electrophoretic lane was 15 µg. Immunoblotting was performed following the Western blot method, as described in [23]. Subsequently, after performing the transference to nitrocellulose membranes, samples homogenized with H Buffer were tested by applying an anti-mouse VEGF antibody (Novus Biologicals; Littelton; CO, USA), whereas those homogenized in the presence of the RIPA buffer were tested by applying an anti-rabbit VEGF-receptor antibody (Novus Biologicals). In both cases, immunoreactivity proteins were detected through subsequent incubation with a peroxidase-conjugated rabbit anti-mouse secondary antibody in the case of the VEGF detection (Dako; Glostrup, Denmark) or with a peroxidase-conjugated donkey anti-rabbit secondary one in the case of VEGF-R (Santa Cruz Biotechnology; Dallas; TX, USA). The utilized dilutions of antibodies were of 1:1000 in the case of both anti-VEGF and anti-VEGF-R, whereas those of secondary ones were of 1:5000. Afterwards, immunoreactivity proteins were shown after development by using a commercial kit (Western Blotting Luminol Reagent; Santa Cruz Technology). Once revealed, the resulted membranes were scanned and stored by digitalization in TIFF format. Then, the same nitrocellulose membranes were subjected to a stripping process in order to remove all antibodies linked to proteins by incubation in an specific stripping buffer containing 10% (v:v) Tween-20®, 1% (w:v) SDS and 15% (w:v) glycine. Incubation in the stripping buffer was conducted for 5 min at 20°C. Afterwards, membranes were washed twice for 10 min in phosphate-Buffered Saline (PBS; pH 7.4), followed by two subsequent washes of 5 min in Tris-Buffered Saline (TBST; pH 8.0). Subsequently, membranes were again subjected to a n immunoblotting detection against α-tubulin as a normalizing protein by using a specific anti-mouse α-Tubulin (Thermo-Scientific; Waltham; MA, USA); which was applied at a dilution of 1:1000. Following incubations with a peroxidase rabbit anti-mouse secondary antibody at a dilution of 1:5000 and subsequent development of specific protein signal was performed as described above for both VEGF and VEGF-R. In all cases, the intensity of the bands was determined by using the Image J Fiji system [24], and both VEGF/α-tubulin and VEGF-R/α-tubulin ratios were calculated after scanning, digitalization, and subsequent storage of α-tubulin results in TIFF format in a similar manner to that described for both VEGF and VEGF-R. Finally, negative controls for VEGF were applied by incubating a randomly chosen 12 months-old prostate sample homogenized in the H Buffer with a specific pre-absorbed VEGF peptide (Novus Biologicals) for 2h at 20°C.This pre-absorbed sample was loaded in a lane of the applied SDS-PAGE together with all other samples. A similar treatment was performed for obtaining a negative control for the VEGF-R, in which a specific pre-absorbed VEGF-R peptide (Novus Biologicals) was also utilized.

Histological and immunohistological staining procedures

As mentioned above, a standard H-E staining procedure was performed to determine the histological architecture in paraformaldehyde-fixed samples. The H-E staining was carried out following the previously well-established procedures as shown in both 5 and 7 µm-thickness slices [25]. Regarding both VEGF and VEGF-R immunohistochemistry analysis, after thawing at room temperature, slides were firstly washed four times with PBS and then permeabilized by incubation with 0.3 (w:v) Triton X-100® in water for 30 min at 20°C. After two further washes with PBS, slides were then blocked through incubation with a 1% (w:v) Serum Bovine Albumin (SBA) solution in PBS for 1h at 20°C. Subsequently, Slides were incubated with the appropriate primary antibodies. In this study, the above-described specific antibodies against VEGF and VEGF-R were utilized at a final dilution of 1:500. Additionally, some slides were co-incubated with the anti-VEGF antibody together with a mouse monoclonal anti-Golgi apparatus antibody (anti-GM130; BD Biosciences; San Jose; CA, USA; catalogue number 610822) at a dilution of 1:500. Incubation with primary antibodies was carried out for 8h at 20°C. Subsequently, slides were washed twice with PBS and the appropriate secondary antibody was added. Thus, to detect the VEGF signal, an Alexa Fluor 488-marked goat-anti mouse secondary antibody (Ref. A11209; Thermo-Fisher Scientific) was utilized, whereas to detect VEGF-R the chosen secondary antibody was an Alexa Fluor 488-marked goat-anti rabbit secondary antibody (Ref. ab 150077; Thermo-Fisher Scientific) and Golgi apparatus was detected by using a FITC-conjugated goat anti-mouse secondary antibody (Ref. ab6785; Abcam; Whaltman; MA, USA). In all cases, dilution of all these secondary antibodies was 1:500 in a 1% (w:v) BSA solution in PBS and samples were incubated for at least 1h at 20°C. Moreover, the nuclear staining Hoechst 33342® (Sigma Aldrich; Santa Cruz; CA,USA) was added together with the utilized secondary antibodies at a final concentration of 1:1000 (v:v). Finally, slides were washed twice with PBS and subsequently mounted by using Mowiol® (Sigma Aldrich). Fluorescence was analyzed through a Zeiss 880 LSM laser confocal microscope (Carl Zeiss Microscopy Gmbh; Jena, Germany) adapted to an inverted Leitz DMIRBE microscope at 63X (N.4 oil; Plan-Apo

Lens; Leitz Gmbh; Stuttgart; Germany). The light source was an argon/krypton laser of 74 mW, whereas fluorescence detection was specifically adapted to each fluorochrome. Images were finally taken and digitalized in TIFF format by using the Microscope Camera Moticam Series 3.0 system (Microptic, S.L.; Barcelona, Spain) for their study.

Statistical analyses

Statistical analyses were carried out through the SPSS 15.0 package for Windows (SPSS Inc., Chicago, IL, USA). First, data were tested for normality and homoscedasticity using the Shapiro–Wilk and Levene tests. Since all data showed normal Gaussian distributions, no transformations were needed. Putative significance of differences was evaluated through a Generalized Estimating Equation (GEE), an extension of Generalized Linear Model (GLM) for repeated measures, which is present in the statistical package. The main characteristics of the GEE were normal distribution and identity link function, whereas the utilized inter-subject factor was age. In all cases, each age was the dependent variable and multiple post hoc comparisons were calculated using Sidak's test. In all statistical analyses, level of significance was set at $P<0.05$. However, since the analytical technique has an intrinsic subjective component, we considered true differences to be only those for which $P<0.05$ and with a percent difference above 20%. Moreover, since both VEGF/α-tubulin and VEGF-R/α-tubulin ratios had arbitrary units, analyses were performed after transforming results taking into consideration that mean values for 1 month-old age rats were 100 and then, values obtained in the other age groups will take 1 month-old group as the baseline.

RESULTS

Histopathological detection of benign prostatic hyperplasia

Histology of prostate glands from 1 month-old rats (prepuberal rats) showed the presence of a tubular ductal epithelium composed by one layer of cuboid epithelial cells surrounded with mesenchymal tissue mainly composed by conjunctival cells and blood vessels (Figures 1A and 1B). Moreover, the presence of a clearly discernible amorphous tubular content positive to the H/E staining was also detected (Figures 1A and 1B). A very similar prostate histological aspect was observed in both 3 months-old rats and 6 months-old ones, although in these cases mean tubular diameters seemed to be greater (Figures 1C and 1D). Additionally, 50% of the analyzed 6 months-old rats showed incipient sings of BPH in the form of focalized ductal areas in which there were more than one layer of epithelial cells (Figure 1D). Finally, epithelial ductal hyperplasia was detected in prostate glands from elder, 12 months-old rats. Hyperplasia was apparent as tubular areas of separate sizes in which there were the accumulation of 2-4 layers of epithelial cells (Figures 1E and 1F). Both the size and the amount of hyperplasia focuses in elder rats were variable, although all of the studied 12 months-old animals showed the presence of hyperplasic areas.

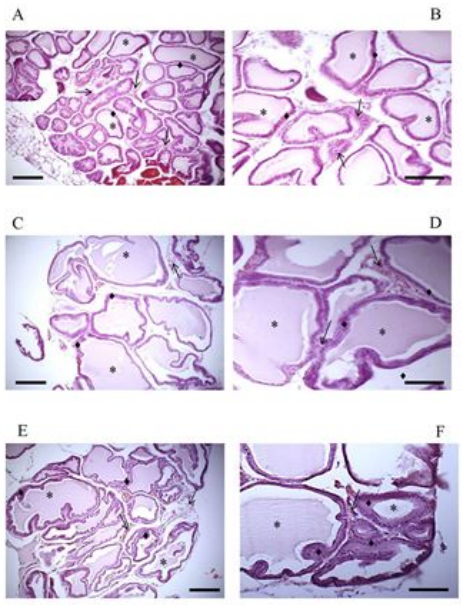

Figure 1: Histological appearance of prostate gland tissues from 1 month-old, 6 months-old and 12 months-old rats.
Note: Prostatic tissues were processed and stained by using the Haematoxylin-Eosin technique as described in the Material and Methods section. A,B: 1 month old rats. C,D: 6 months-old rats. E,F: 12 months-old rats. A,C,E: images observed at 100X magnification. B,D,F: images observed at 1000X magnification. *: intraductal areas: interstitial tissue. •: ductal epithelium. Bars in images A, C and E indicate 100 μm length, whereas bars in images B, D and F indicate 20 μm length. Figure shows representative images obtained from seven 1 month-old rats, seven 6 months-old animals and seven 12 months-old ones.

Expression and location of VEGF in prostate tissue from rats of separate ages

Western blot analyses showed the presence of a specific 42 kDa band in prostatic samples from prepuberal rats which corresponded to the presence of VEGF (Figure 2A). The analysis of the relative intensity of this band did not show any significant difference in this parameter when compared 1 month-old rats and 3 months-old ones (Figure 2B). On the contrary, both 6 months-old rats and 12 months-old ones showed a significant ($P<0.05$) increase in the relative intensity of the prostate VEGF band, which was especially intense in the oldest animals (199.6 ± 4.4, arbitrary units in 12 months-old rats *vs.* 100.0 ± 1.4, arbitrary units, in 1 month-old ones; see Figure 2B). Specific prostate immunohistochemistry showed a perimembranous location in prostatic ductal cells of VEGF in 1 month-old rats (Figure 2C). This distribution was progressively migrating to cellular cytoplasm with age (Figure 2D), reaching to a very noticeable cytoplasmic VEGF location in 12 months-old animals (Figure 2E). Cytoplasmic VEGF signal was often observed as vesicle-like forms (Figures 2D and 2E). Additionally, some ductal cells in 12 months-old animals showed an intense VEGF marking linked with the Golgi apparatus (Figure 2F).

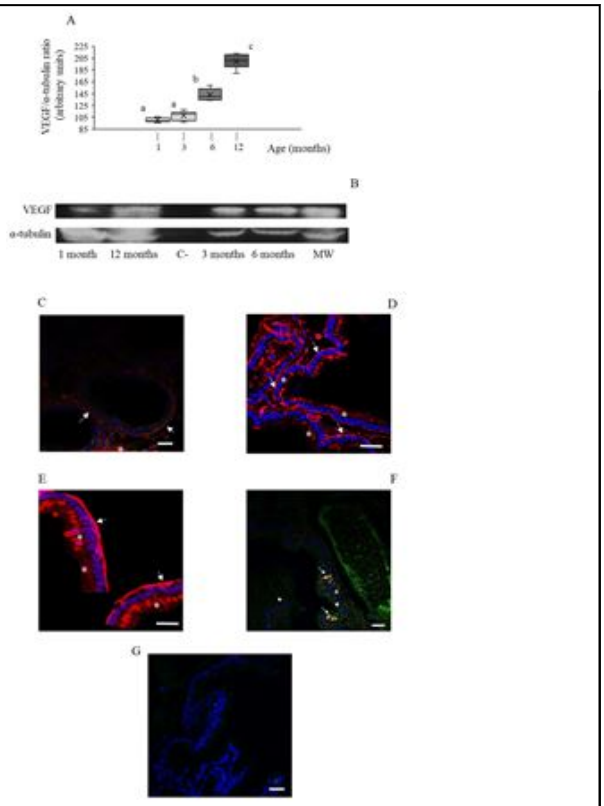

Figure 2: Expression and intracellular location of VEGF receptor in prostatic tissues from rats of separate ages.

All procedures have been described in the supplied Supplementary Material. A: box and whisker plot representation of obtained VEGF-R/α-tubulin ratio through the Western blot procedure. White bars: prepuberal rats. Light grey bars: young rats. Dark grey bars: adult rats. Black bars: elder rats. Asterisks indicate significant ($P<0.05$) differences when compared with the prepuberal group. Results showed data dispersion, S.E.M, means (intra-box continuous line) and median (intra-box discontinuous line) for 7 rats in each age group. B: representative image of the specific VEGF-R band obtained after the Western blot analysis and revealed as negative image. VEGF-R: VEGF-R lane; α-tubulin: concomitant α-tubulin lane. Image is representative for the analysis of 7 animals in each age group. C-E: immunocytochemistry against VEGF-R. C: prepuberal rats. D: adult rats. E: elder rats. F: negative control for the utilized primary antibodies. All images are shown at 1000X magnification. Arrows point out VEGF-R-positive markings. Bars indicate 100 μm lengths.

Expression and location of VEGF receptor in prostatic tissue

Likewise to that observed with VEGF, Western blot analyses of prostatic tissues from 1month-old rats showed the presence of a specific 222 kDa band corresponding to the presence of the VEGF receptor (Figure 3A). There were no significant differences in the relative intensity of the VEGF receptor band among 1 month-old rats, 3 months-old animals and 6 months-old ones (Figure 3B). Conversely, 12 months-old rats underwent a significant ($P<0.05$) increase in the VEGF receptor relative intensity band, reaching values of 146.9 ± 10.7, arbitrary units (as comparison, 100.0 ± 4.3, arbitrary units, in 1 month-old rats; see Figure 3B). Regarding the location, immunohistochemistry showed the presence of VEGF receptor in both per membranous and cytoplasmic locations in all analyzed age groups, without noticeable changes in its location (Figures 3C and 3E).

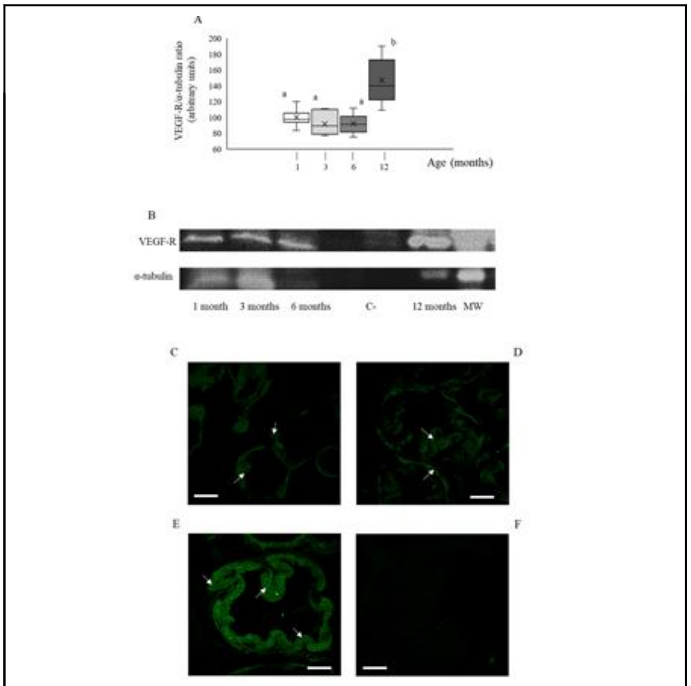

Figure 3: Expression and intracellular location of VEGF in prostatic tissues from rats of separate ages.

All procedures have been described in the supplied Supplementary Material. A: box and whisker plot representation of obtained VEGF/α-tubulin ratio through the Western blot procedure. White bars: prepuberal rats. Light grey bars: young rats. Dark grey bars: adult rats. Black bars: elder rats. Asterisks indicate significant ($P<0.05$) differences when compared with the prepuberal group. Results showed data dispersion, S.E.M, means (intra-box continuous line) and median (intra-box discontinuous line) for 7 rats in each age group. B: representative image of the specific VEGF band obtained after the Western blot analysis and revealed as negative image. VEGF: VEGF lane; α-tubulin: concomitant α-tubulin lane. Image is representative for the analysis of 7 animals in each age group. C-E: immunocytochemistry against VEGF. C: prepuberal rats. D: adult rats. E: elder rats. F: VEGF-Golgi apparatus co-location in elder rats. G: negative control for the utilized primary antibodies. All images are shown at 1000X magnification. Asterisks indicate VEGF-positive intracytoplasmic markings, whereas arrows point out VEGF-positive per membranous ones. Arrows in F: positive VEGF-Golgi apparatus co-location. Arrowheads: nucleuses. In all images, blue spots indicate cell nucleuses stained through the Hoechst 33342® technique. Bars indicate 100 μm length.

DISCUSSION

Results shown in this work suggest that the onset of BPH is related with specific changes in the expression and location of VEGF, which started before the appearance of evident histological signs of hyperplasia. These changes would lead to an increase in both prostate, Golgi apparatus-related VEGF processing and further extracellular secretion. Furthermore, our results concerning VEGF-R and Golgi apparatus co-location also suggest that these changes could be modulated by both canonical and non-canonical mechanisms. In this way, vasculogenesis-related mechanisms that were at least partially modulated by VEGF could be one of the mechanisms involved in the onset of BPH. Our results indicated that changes in the intracellular expression and distribution of VEGF seem to be more important than those of VEGF-R would be more important as mechanisms involved in the onset of BPH. In fact, VEGF-R expression only increased in 12 months-old rats, in which BPH was already established. Thus, results suggest that an increase in VEGF-R levels would not be related with the onset of BPH. On the3 contrary, there is a noticeable location change of VEGF from perimembranous areas in pre-pubertal (1 month-old rats) and young animals (3 months-old) to intracellular ones, linked to Golgi apparatus in older individuals. It is noteworthy that, according to our knowledge, the perimembranous location of VEGF has not been described before in prostatic tissue. This is different to that described for other pathologies such as renal carcinoma, in which VEGF appeared in both cytoplasmic and per membranous areas [26,27]. Otherwise, the appearance of VEGF signal linked to Golgi apparatus not only would suggest the existence of a non-canonical pathway for VEGF, but also the appearance of post-translational changes in intracellular VEGF. Considering all these results, it would be reasonable to suggest that the observed changes in VEGF location in 12 months-old rats could be also related with the appearance of VEGF-Golgi apparatus co-location. In this sense, it is interesting to remind that there are several reports indicating that changes in intracellular location of Golgi apparatus have been related with the onset of tumoralprocesses in tissues such as colon, stomach, and mammary gland [28-30]. Therefore, our results suggest that the onset and subsequent establishment of BPH would be related with an increase in the expression of VEGF that could lead to angiogenic alterations leading to the appearance of ill-regulated cell prostate proliferation.

CONCLUSION

Data showed here suggest that the onset of age-related benign prostatic hyperplasia (BPH) is concomitant with an increase of intracellular levels of VEGF. This increase was concomitant with a re-distribution of VEGF intracellular location that, in turn, was parallel with an increase in VEGF-Golgi apparatus co-location. These changes would lead to angiogenic alterations in prostate tissue that would be one of the factors involved in further development of prostatic tumors in rats.

DISCLOSURE AND CONFLICT OF INTERESTS ESTATEMENT

No disclosure was applicable on this work. Likewise, there is no conflict of interest related with this manuscript. Furthermore, no specific Funding was afforded for this work.

REFERENCES

1. Golomb E, Rosenzweig N, Eilam R, Abramovici A. Spontaneous hyperplasia of the ventral lobe of the prostate in aging genetically hypertensive rats. J Androl. 2000;21:58-64.
2. Mahapokai W, Sluijs VF, Schalken J. Models for studying benign prostatic hyperplasia. Prostate Cancer. 2000;3:28-33.
3. Lepor H. Pathophysiology, epidemiology and natural history of benign prostatic hyperplasia. Rev Urol. 2004;6:S3-S10.
4. Cheng I, Witte JS, Jacobsen SJ, Haque R, Quinn VP, Quesenberry CP, et al. Prostatitis, sexually transmitted diseases, and prostate cancer: The california men's health study. PLoS One. 2010;5:e8736.
5. Kopp RP, Freedland SJ, Parsons JK. Associations of benign prostatic hyperplasia with prostate cancer: The debate continues. Eur Urol. 2011;60:691-698.
6. Ørsted DD, Bojesen SE, Nielsen SF, Nordestgaard BG. Association of clinical benign prostate hyperplasia with prostate cancer incidence and mortality revisited: A nationwide cohort study of 3009258 men. Eur Urol. 2011;60:691-698.
7. Gurel B, Lucia MS, Thompson IM, Goodman PJ, Tangen CM, Kristal AR, et al. Chronic inflammation in benign prostate tissue is associated with high-grade prostate cancer in the placebo arm of the prostate cancer prevention trial. Cancer Epidemiol Prevent Biomark. 2014;23:847-856.
8. Dai X, Fang X, Ma Y, Xianyu J. Benign prostatic hyperplasia and the risk of prostate cancer and bladder cancer: A meta-analysis of observational studies. J Medicine. 2016;95:e3493.
9. Nascimento-Gonçalves E, Colaço B, Ferreira R, Oliveira PA. Human and animal prostate cancer similarities and differences: Models to study this disease. Life Sci. 2018;203:210-224.
10. Bostanci Y, Kazzazi A, Momtahen S, Laze J, Djavan B. Correlation between benign prostatic hyperplasia and inflammation. Curr Opin Urol. 2013;23:5-10.
11. Gandaglia G, Briganti A, Gontero P, Mondaini N, Novara G, Salonia A, et al. The role of chronic prostatic inflammation in the pathogenesis and progression of Benign Prostatic Hyperplasia (BPH). BJU Int. 2013;112:432-441.
12. Zhang M, Luo C, Cui K, Xiong T, Chen Z. Chronic inflammation promotes proliferation in the prostatic stroma in rats with experimental autoimmune prostatitis: Study for a novel method of inducing benign prostatic hyperplasia in a rat model. World J Urol. 2020a;38:2933-2943.
13. Zhang L, Wang Y, Qin Z, Gao X, Xing Q, Li R, et al. Correlation between prostatitis, benign prostatic hyperplasia and prostate cancer: Asystematic review and meta-analysis. J Cancer. 2020b;11:177-189.
14. De-Nunzio C, Kramer G, Marberger M, Montironi R, Nelson W, Schröder F, et al. The controversial relationship between benign prostatic hyperplasia and prostate cancer: The role of inflammation. EurUrol. 2011;60:106-117.
15. Huss WJ, Hanrahan CF, Barrios RJ, Simons JW, Greenberg NM. Angiogenesis and prostate cancer: identification of a molecular progression switch. Cancer Res. 2001;61:2736-2743.
16. Duffy AM, Bouchier-Hayes DJ, Harmey JH. Vascular Endothelial Growth Factor (VEGF) and its role in non-endothelial cells: Autocrine signalling by VEGF. Curie Bio Sci. 2013.

17. Mukherjee P, Sotnikov AV, Mangian HJ, Zhou JR, Visek WJ, Clinton SK. Energy intake and prostate tumor growth, angiogenesis, and vascular endothelial growth factor expression. J Nat Cancer Inst. 1999;91:512-523.
18. Eisermann K, Fraizer G. The androgen receptor and VEGF: Mechanisms of androgen-regulated angiogenesis in prostate cancer. Cancers. 2017;9:32-42.
19. Trujillo-Rojas L, Fernández-Novell JM, Blanco-Prieto O, Rigau T, Rivera del Álamo MM, Rodríguez-Gil JE. The onset of age-related benign prostatic hyperplasia is concomitant with increased serum and prostatic expression of VEGF in rats: Potential role of VEGF as a marker for early prostatic alterations. Theriogenology. 2022.
20. Neufeld G, Cohen T, Gengrinovitch S, Poltorak Z. Vascular Endothelial Growth Factor (VEGF) and its receptors. FASEB J. 1999;13:9-22.
21. Bradford MM. A rapid and sensitive method for the quantitation of microgram quantities of protein utilizing the principle of protein-dye binding. Anal Biochem. 1976;72:248-254.
22. Laemmli UK. Cleavage of structural proteins during the assembly of the head of bacteriophage T4. Nature. 1970;227:680-685.
23. Burnette WN. Western blotting: Electrophoretic transfer of proteins from sodium dodecyl sulfate–polyacrylamide gels to unmodified nitrocellulose and radiographic detection with antibody and radioiodinated protein A. Anal Biochem. 1981;112:195-203.
24. Schindelin J, Arganda-Carreras I, Frise E, Kaynig V, Longair M, Pietzsch T, et al. Fiji: An open-source platform for biological-image analysis. Nature Meth. 2012;9:676-682.
25. Little TV, Holyoak GR. Reproductive anatomy and physiology of the stallion. Vet Clin N Am Equine. 1992;8:1-29.
26. Djordjevic G, Mozetic V, Mozetic DV, Licul V, Ilijas KM, Mustac E, et al. Prognostic significance of vascular endothelial growth factor expression in clear cell renal cell carcinoma. Pathol Res Pract. 2007;203:99-106.
27. Matušan-Ilijaš K, Babarović E, Hadžisejdić I, Grahovac M, Grahovac B, Jonjić N. Hypoxia inducible factor-1α correlates with vascular endothelial growth factor A and C indicating worse prognosis in clear cell renal cell carcinoma. J Exp Clin Cancer Res. 2009;28:40-43.
28. Xie B, Tam N, Tsao S, Wong Y. Co-expression of Vascular Endothelial Growth Factor (VEGF) and its receptors (flk-1 and flt-1) in hormone-induced mammary cancer in the Noble rat. Brit J Cancer. 1999;81:1335-1343.
29. Waldner MJ, Wirtz S, Jefremow A, Warntjen M, Neufert C, Atreya R,et al. VEGF receptor signaling links inflammation and tumorigenesis in colitis-associated cancer. J Exp Med. 2010;207:2855-2868.
30. Lian L, Li XL, Xu MD, Li XM, Wu MY, Zhang Y, et al. VEGFR2 promotes tumorigenesis and metastasis in a pro-angiogenic-independent way in gastric cancer. BMC Cancer. 2019;19:1-15.